Rev. Adv. Mater. Sci. 45 (2016) 84-90

SYNTHESIS OF SILICON HOLLOW NANOSPHERES WITH A MESOPOROUS SHELL VIA A LOW-TEMPERATURE METATHESIS REACTION

Hao Liu[1,2], Haokun Deng[3], Jian-Qiang Bi[4,5] and Katerina E. Aifantis[6]

[1]Center for Composite Materials, University of Delaware, Newark, DE 19716, USA
[2]Department of Mechanical Engineering, University of Delaware, Newark, DE 19716, USA
[3]Department of Materials Science and Engineering, The University of Arizona, Tucson, AZ 85721, USA
[4]Key Laboratory for Liquid-Solid Structure Evolution and Processing of Materials (Ministry of Education), Shandong University, Jinan 250061, China
[5]Engineering Ceramics Key Laboratory of Shandong Province, Shandong University, Jinan 250061, China
[6]Department of Civil Engineering and Engineering Mechanics, The University of Arizona, Tucson, AZ 85721, USA

Received: April 30, 2016

Abstract. Over the past years significant focus has been given on fabricating nanomaterials with unique shapes and structures. This article presents a new configuration for Si nanoparticles that have a hollow structure, whose shell contains mesopores. These structures were obtained through a simple chemical method by using $SiCl_4$ with Zn as the reactant and solvent. The coupling effects between the buoyancy, surface tension, and diffusion of $ZnCl_2$ are responsible for the formation of the hollow structures, with a high production rate and quality. Characterization of the resulting powders, through X-ray diffraction, transmission electron microscopy and Raman spectroscopy, illustrated that the diameter of the hollow Si nanospheres ranged from 150 nm to 300 nm, while nitrogen adsorption and density functional theory calculations indicated that their surface area was 193.498 m^2/g and mesopores 2-4 nm in diameter existed in their shell.

1. INTRODUCTION

With the advancement of nanotechnology the development of Si nanostructures has been extensively pursued for multiple applications. Numerous novel silicon nanostructures have been synthesized, such as silicon nanotubes [1–5], nanowires [6–12], nanorods [13,14], nanodots [15–17], nanopillars [18,19], and nanospheres [20,21], to name a few. Due to their unique mechanical, optical, electron transport properties, field emission characteristics, and excellent thermal conductivity, silicon materials promise to have a wide range of applications in numerous fields, such as: solar cells [22], Li-ion batteries [23], biosensors [24], photodetectors [25], luminescent labels to DNA [26], hydrogen storage [27], and cell separation [28].

Depending on the application a different nanostructure must be employed; for example for solar cells arrays of Si patterned surfaces must be used [22], whereas for anodes of Li-ion batteries Si hollow nanospheres (SHNs) are the more promising [29]. A method to further improve capacity retention of these hollow nanospheres would be to make their shell porous, since it has been observed that porous Si foams possess both a high capacity and high coulombic efficiency [30]. This preferred performance of porous Si can be due to the higher surface area available for Li-ions to diffuse through (and hence lithiate a larger portion of the Si) and

Corresponding author: Katerina E. Aifantis, e-mail: kaifanti@mtu.edu

also the ability of the porous structure to withstand the 400% volume expansions that Si experiences upon lithiation.

To the best of our knowledge, very few efficient methods for producing silicon hollow nanospheres with low costs have been developed, and none of these result in a porous shell. This is a drawback if one compares with the significant progress that has been made in synthesizing and utilizing for other materials chemistries including carbon [31–34], SnO_2 [35–38], and PbS hollow nanospheres [39,40]. The routes developed for the synthesis of nanomaterials include physical, chemical and electrochemical techniques, which can be categorized as (i) one step template-free chemical synthesis used for fabrication of SnO_2 [35,37] and PbS hollow nanostructures [39], (ii) adding copper sulfide (CuS) nanocrystals and monophenylsilane (MPS) to supercritical toluene to fabricate Si nanowires [41], and (iii) the template replication method combining a CVD process to fabricate Si nanowires [42] and interconnected Si hollow nanospheres [43]. Despite their effectiveness, most of these procedures suffer from the high temperatures required, the special catalyst or template necessary for the reactions to take place, longer reaction time, poorer purity, or higher costs that cannot be ignored. In the sequel, therefore, a novel route to prepare silicon nanospheres with a high purity and high productivity is presented. The solid-state metathesis (SSM) reactions have been proved to be a simple and effective route to obtain hollow metal carbides, nitrides, silicides, borides, pnictides, and chalcogenides, as well as ternary phases, and therefore will be employed in the sequel.

2. MATERIAL AND METHODS

2.1. Materials and synthesis

Liquid $SiCl_4$ (99%, ACS reagent), HCl(37%, ACS reagent) were purchased from Sigma Aldrish. Zn powders (99%, particle size 1-10 μm, AR) were purchased from Aladdin Chemistry Co. Ltd. All reactants were used as obtained. The mixture of 3 mL of $SiCl_4$ and 15 g Zn powders was loaded to a 316L stainless steel reaction autoclave with a 30 mL capacity. $SiCl_4$ was the Si source and Zn powders were the reducing agent. Zn powders also acted as the metallic solvent due to its low melting point (419.58 °C) compared to the higher reaction temperature and its good solubility (soluble in both acid and alkali solutions). It is expected that during the heating process the higher density of liquid Zn (ρ = 7.14 g/mL) will lead to a higher buoyancy which will aid the separation of the solid reaction products from the raw materials according to the Archimedean principle. Before the autoclave was sealed and heated, degasification was done by allowing N_2 to flow through the autoclave chamber for sufficient time to prevent side reactions such as oxidation caused by the oxygen in the air. Then the autoclave with reactants was sealed carefully and heated to 530 °C in an electric oven for 8 h to ensure sufficient reaction time. Then the autoclave was cooled down to room temperature and was unsealed to collect the reaction products. The reaction products were washed with hydrochloric acid (HCl) and deionized water (DI water) several times to completely remove residual reactants and impurities. Then the washed products were dried for 10 h at 50 °C in vacuum.

2.2. Materials and chemical characterization

X-ray diffraction was performed using a Rigaku Dmax-rc X-ray diffractometer (XRD) with Ni filtered Cu K_α radiation (V = 40 kV, I = 50 mA) at a scanning rate of 4°/min. The morphology of the Si nanostructures was examined through a Hitachi H-800 transmission electron microscope (TEM) and a JEOL JEM-2100 high-resolution transmission electron microscope (HRTEM). Fourier transformation infrared (FTIR) spectroscopy was also conducted on a Bruker VERTEX 70 spectrometer. The nitrogen adsorption and desorption isotherms were obtained at 77K through a Quadrasorb SI sorption analyzer to examine the porosity. The specific surface area was calculated based on the Brunauer-Emmett-Teller (BET) model and the pore size distribution of the mesopores which might possibly appear on the surface of the silicon nanospheres was calculated from the desorption data through the use of the Density Functional Theory (DFT) method. The details of the DFT theory model for calculating the pore size distribution were introduced elsewhere [44].

3. RESULTS AND DISCUSSION

Fig. 1 depicts the XRD pattern of the as-prepared sample. It is seen that the strong peaks denote face-centered cubic Si (space group Fd-3m) with a lattice constant of a = 5.438 Å, which is consistent with the JCPDS card No. 27-1402 within experimental error. The several weak background peaks are due to the existence of residual Zn and SiO_2 from the native oxidation layer of Si. The relative intensity of

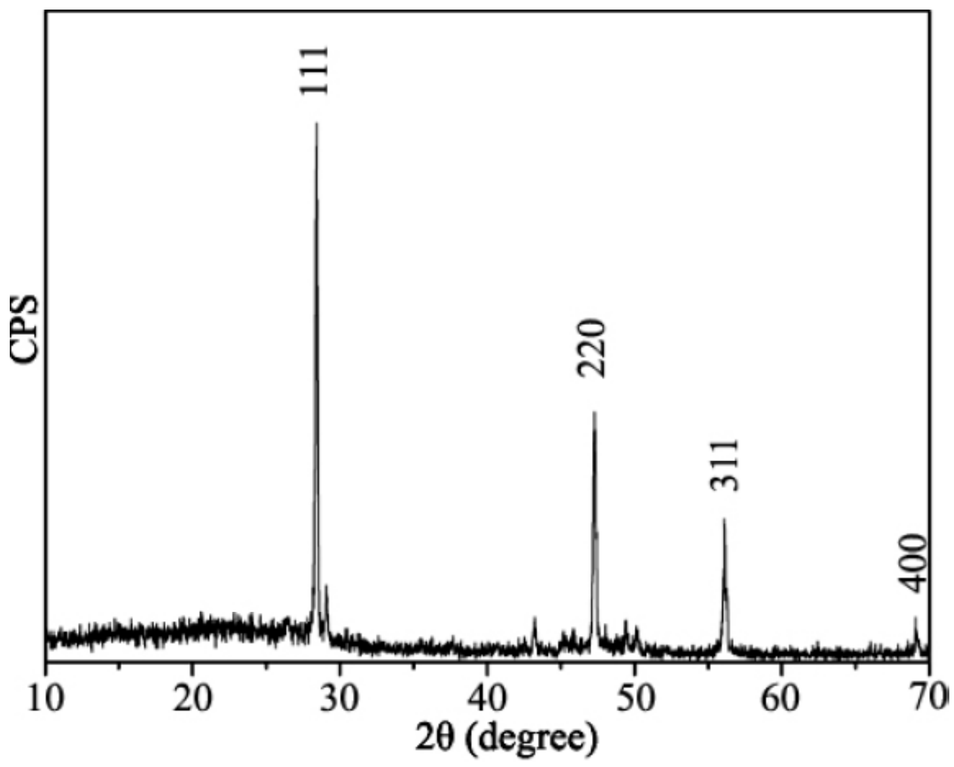

Fig. 1. XRD pattern of the products obtained by the reaction of $SiCl_4$ and Zn. The 111, 220, 311, and 400 peaks correspond to Si.

these peaks indicates that the content of residual Zn is very low.

The detailed IR experiment performed on samples was employed to further determine the composition of the products. As shown in Fig. 2, the three peaks located at 459.51, 798.26, and 1080.22 cm^{-1} correspond to the characteristic Si-O-Si bond, Si-O-Si symmetric stretch, and Si-O-Si anti-symmetric stretch, respectively. In addition, the peak at 940.24 cm^{-1} matches with the Si-O-H stretch [45]. Also, according to the Si-OH vibrational mode [46], the band at 1629.80 cm^{-1} can be attributed to the hydroxyl groups that are bound to the surface of the Si. The large amount of O_2 and H_2O existing under the reaction temperature in the experimental process can passivate the surface of the SHNs with oxide and hydroxide [47].

Fig. 3 displays some representative TEM images of the obtained products, which provide clear and detailed information about the obtained nanostructures. As shown in Figs. 3a, 3b, 3c, and 3d, the homogeneous Si quasi-spherical particles have diameters in the range of 150~300 nm, and tend to agglomerate but maintain their individual structure. The strong contrast between the dark edge and the relatively bright center indicates their hollow nature, which is also obviously illustrated in Figs. 3e and 3f. The electron diffraction pattern of a selected area of the obtained nanoparticles is exhibited in Fig. 3e, which verifies the formation of face-centered cubic Si. The HRTEM image in Fig. 3f reveals the outer shell and inner part of a SHNs from which it can be seen that the shell thickness is about 13 nm. The clear lattice fringes give a spacing of 0.31 nm between adjacent planes, coinciding well with the information about of the (111) plane of the face-centered cubic silicon. It should be noted that the non-uniformity in contrast of the surface of the SHNs shows that subtle substructures exist on the shell, namely mesopores.

To examine mesopores on the surface of SHNs, nitrogen sorption behavior analysis was conducted and Fig. 4 illustrates the nitrogen adsorption/desorption isotherms and the DFT pore-size distribution curve. The isotherms in Fig. 4a show a hysteresis characteristic of the type II isotherms, which

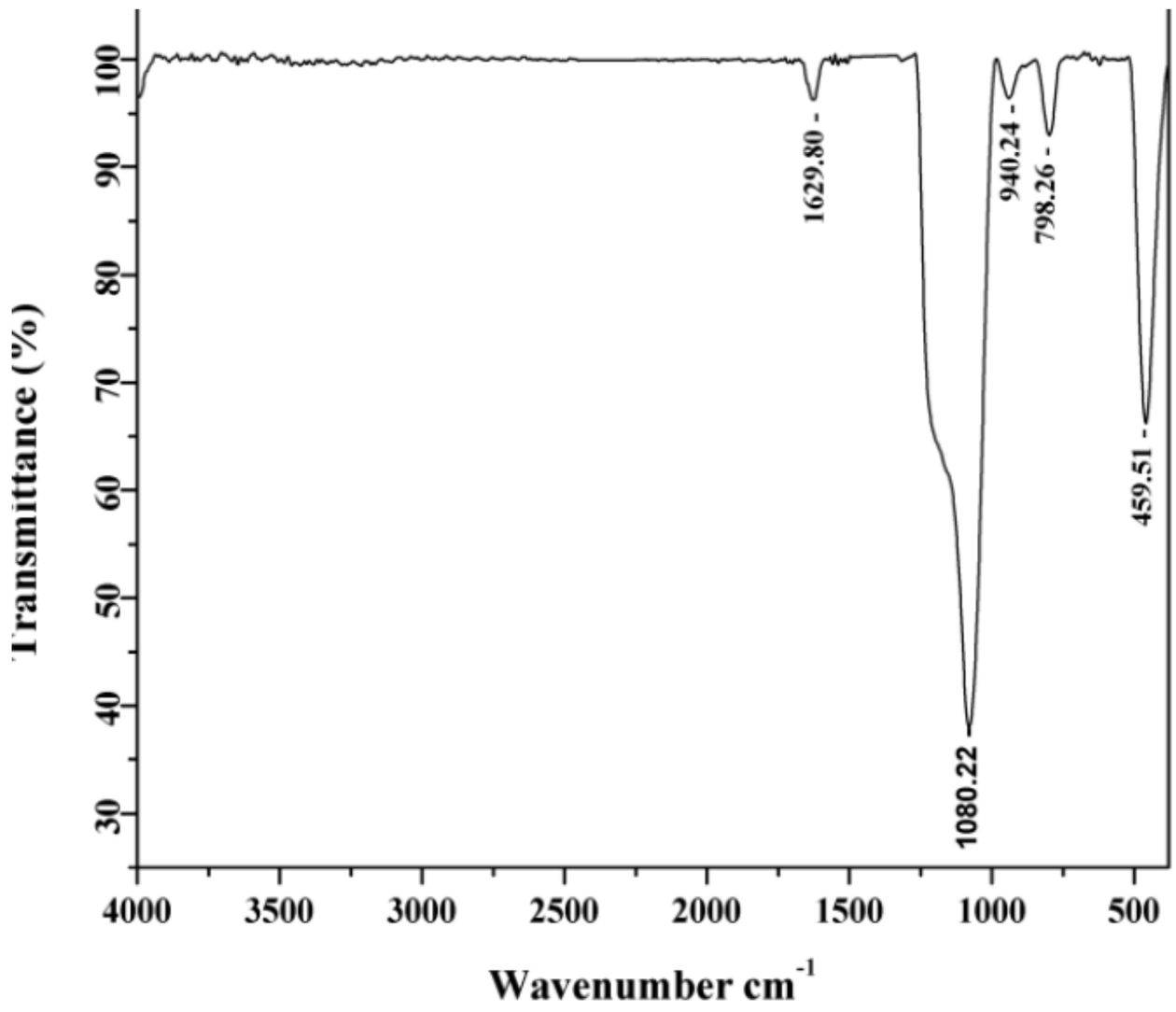

Fig. 2. FTIR spectrum of the collected products.

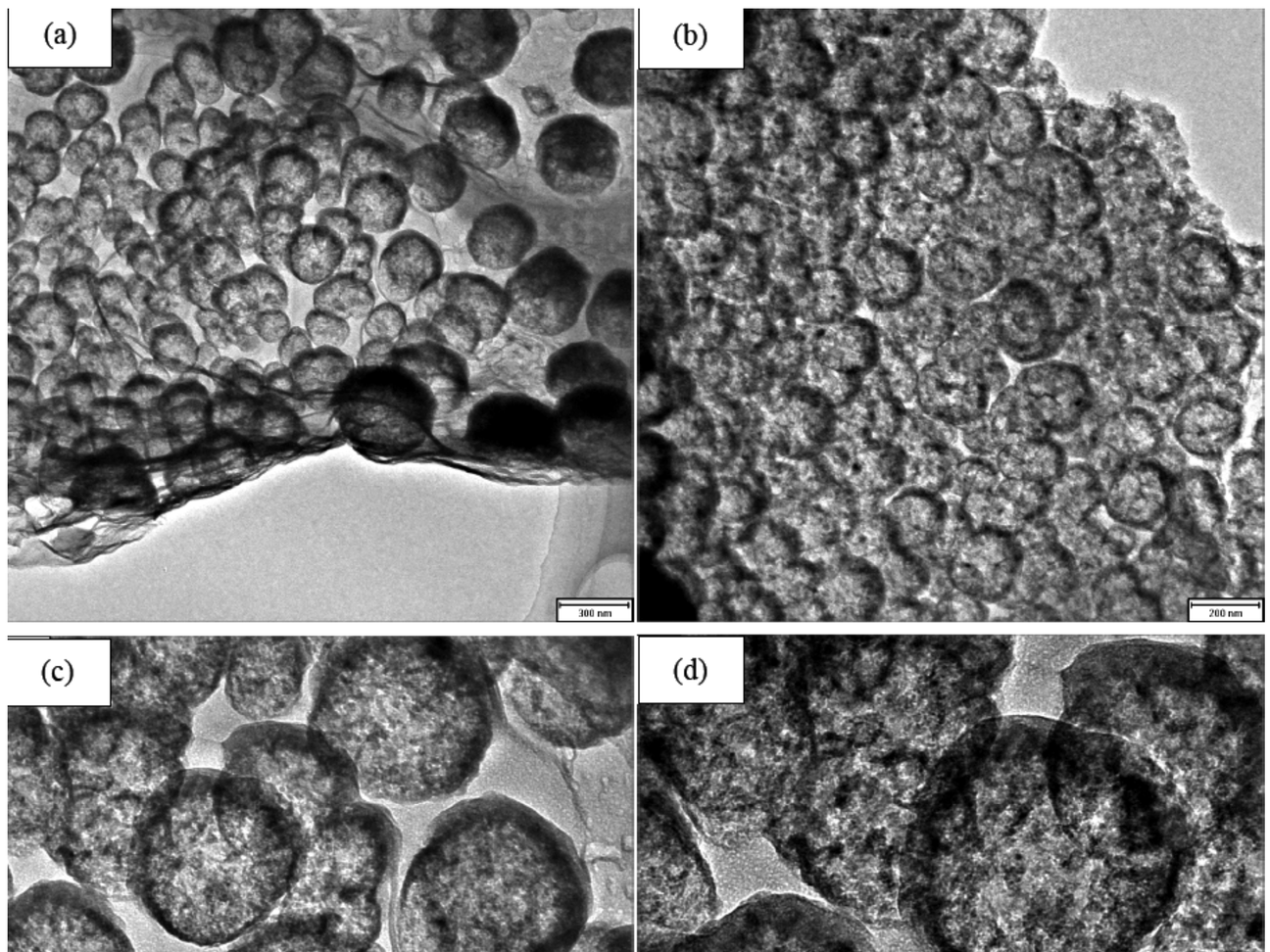

Fig. 3. Representative TEM images of the obtained products. (a), (b), (c), and (d) showed the general view of the agglomerated silicon hollow spheres. (e) illustrates the electron diffraction pattern of a selected area in (a)~(d). (f) is the HRTEM image of the surface of a silicon hollow sphere.

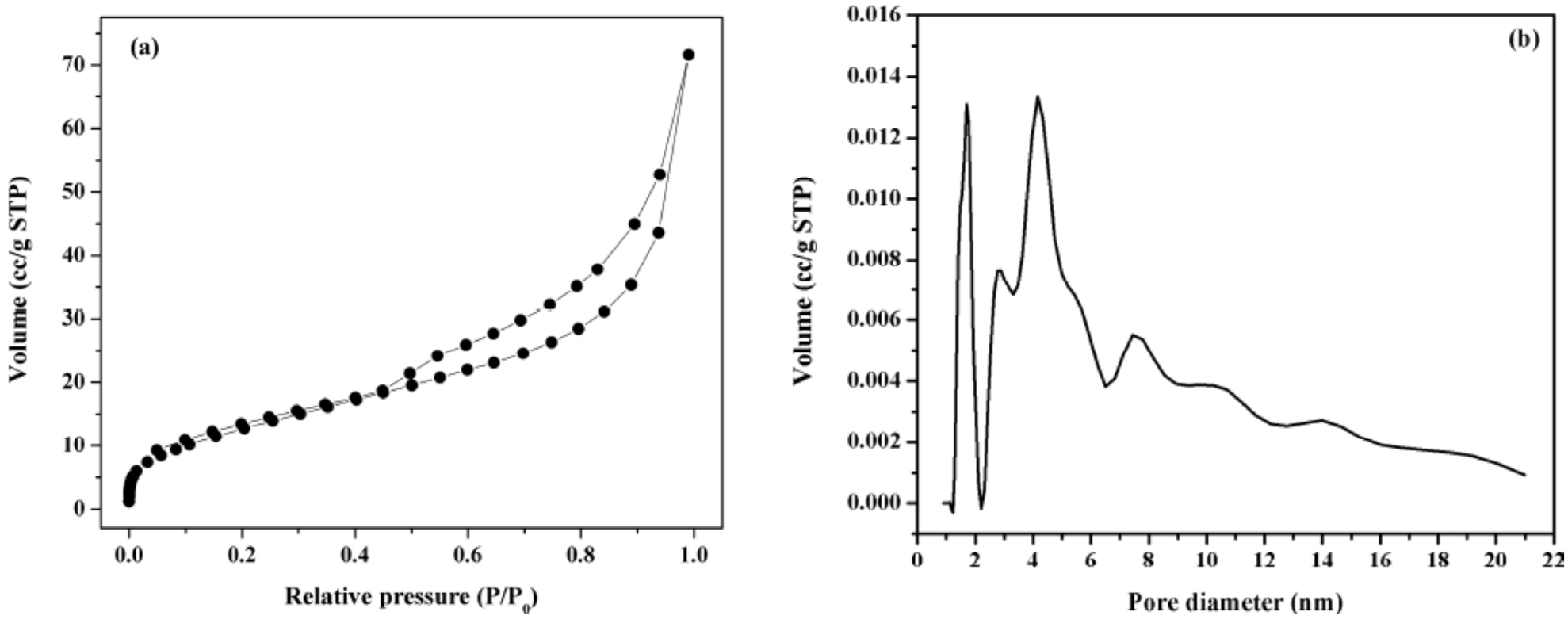

Fig. 4. (a) Nitrogen adsorption/desorption isotherms and (b) DFT pore-size distribution curve determined from the nitrogen desorption isotherm on the obtained SHNs.

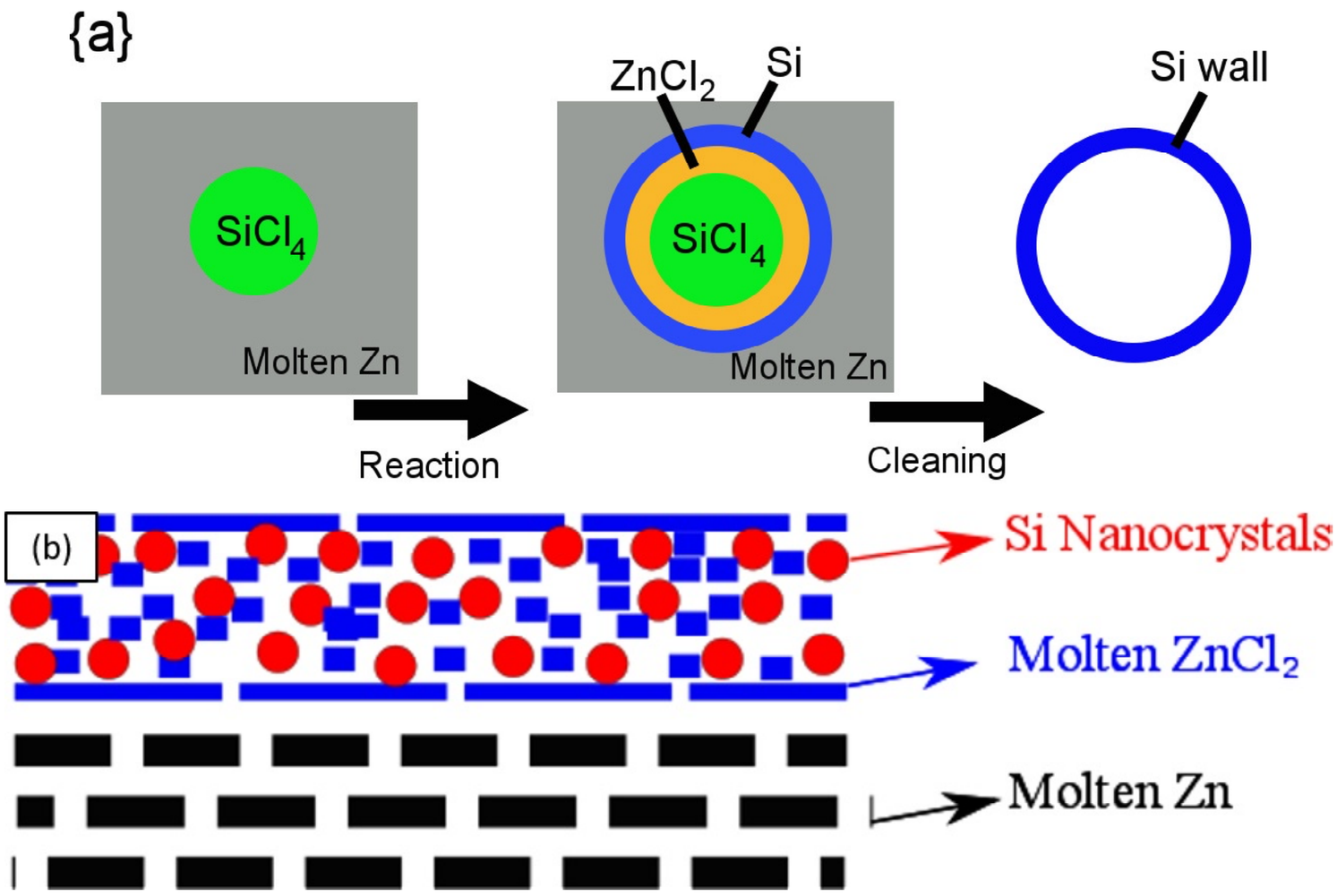

Fig. 5. Schematic illustration of (a) formation mechanism of the SHNs, and (b) the layered configuration indicating the buoyancy effect.

suggests the existence of the mesopores in the obtained products [48]. The pore size distribution of the SHNs is evaluated based on the DFT method and the two most obvious distribution peaks shown in Fig. 4b correspond to the pores primarily around 2 nm and 4 nm. The BET surface area of SHNs calculated from the results of nitrogen adsorption is 193.498 m^2/g. The existence of the mesopores demonstrated by nitrogen adsorption and DFT pore-size calculation well explains the non-uniform contrast on the SHNs in the TEM images and the pore-like morphology.

Herein, we also present a simple but robust mechanism for the formation of SHNs using the SSM reactions. At the first stage of the fabrication process, the liquid $SiCl_4$ rapidly vaporized when the temperature reached the boiling point of $SiCl_4$, which is 57.6 °C, resulting in an increase in the pressure inside the autoclave, which was estimated to be about 12 MPa. As the temperature kept increasing to 419.5 °C, another phase transformation, which was the melting of solid Zn, started to take place. Due to the high pressure an increasing amount of $SiCl_4$ dissolved into the liquid Zn. The $SiCl_4$ vapor entered the liquid Zn through the liquid-gas interface and it was able to form spherical cavities in the liquid Zn due to the surface tension. The high Laplace pressure that resulted from the surface tension of the liquid-gas interface allowed the $SiCl_4$ vapor cavities to achieve a nanoscale size. Since the temperature was much higher than the liquid-vapor critical temperature (235 °C) of $SiCl_4$, the $SiCl_4$ vapor cavities were able to exist stably.

As the temperature further increased to 530 °C, the redox reaction between Zn and $SiCl_4$ was fully activated at the spherical liquid-gas interface. The process is schematically illustrated in Fig. 5a. Once the bonds between the Si and Cl were broken, the four valence electrons of each Si atom formed covalent bonds with neighboring Si atoms. Once the reaction between $SiCl_4$ and Zn initiated, the appearance of the Si was accompanied with the formation of $ZnCl_2$ whose melting point is around 290 °C. During the formation of $ZnCl_2$ a significant amount of instantaneous heat was released by the highly exothermic reaction (ΔH_f° = -173.1 kJ mol^{-1}), increasing the amount of Zn that melted and further enhancing the chemical reaction between $SiCl_4$ and Zn. This resulted in the formation and accumulation of a significant amount of Si and $ZnCl_2$ at the spherical interface between the nanosized $SiCl_4$ cavities and the liquid Zn, as shown in Fig. 5a.

The Si formed according to the following chemical metathesis reaction:

$$SiCl_4 + 2\,Zn \rightarrow Si + 2\,ZnCl_2,$$

$$\Delta G = -16.3 \text{ kcal/mole (at } T = 823\,\text{K}).$$

The accumulating Si layer became dense and uniform, and eventually attained a hollow structure when $SiCl_4$ inside the cavity was completely consumed. The Si layer and $ZnCl_2$, together, prevented further reaction between Si and $ZnCl_2$, although the reaction might still take place at a low rate, considering the porosity of the Si layer, which provided paths for $SiCl_4$. The densities of Si, $ZnCl_2$, and Zn are 2.33,

2.907 and 7.14 g/mL respectively, therefore the multi-shell Si-Zn nanoparticles floated upwards into the liquid $ZnCl_2$ due to the buoyancy which resulted from the difference in density, as shown in Fig. 5b. The buoyancy effect provided by $ZnCl_2$ separated the Si-Zn nanoparticles and prevented them from clustering, maintaining the nano-size of the particles. Then the $ZnCl_2$ and the solidified Zn that remained around the Si shell were removed by washing with hydrochloric acid and DI water, leaving the Si hollow nanospheres.

5. CONCLUSIONS

A simple metathesis reaction between Zn and $SiCl_4$ at 530 °C was employed to fabricate novel Si hollow nanospheres (150-300 nm in diameter) with a mesoporous shell. Zn acted as both the reactant and metallic solvent and the coupling effect of the buoyancy, surface tension, and diffusion of $ZnCl_2$ and Si atoms is responsible for the formation of the hollow structure. Furthermore, TEM images revealed the existence of mesopores on the Si shell, resulting in a high surface area (193.498 m^2/g). This "double-porosity" structure, of the hollow spheres with mesoporous shells, is promising for numerous application, such as in anodes for Li-ion batteries where porous structures optimize Li-ion diffusion and accommodate the Si volume expansions.

ACKNOWLEDGEMENTS

This work was financially supported by the National Natural Science Foundation of China (No. 50872072, 51042005, and 50972076), Science and Technology Development Project of Shandong Province (2009GG10003001 and 2009GG10003003), Fund for Outstanding Young Researchers of Shandong Province (2007BS04048), Independent Innovation Foundation of Shandong University, and National Innovative Experiment Program for University Students in China (No. 091042213 in Shandong University). The authors thank Zheng Zhang, Lei Yan, Xiaojing Li, Suhong Liu, and Chen Sui in School of Material Science and Engineering and Key Laboratory for Liquid-Solid Structure Evolution and Processing of Materials (Ministry of Education), Shandong University, Jinan 250061, China, for helpful advice on the design and characterization of experiments. No conflict of interest is declared.

REFERENCES

[1] J. Lan, D. Cheng, D. Cao and W. Wang // *J. Phys. Chem. C.* **112** (2008) 5598.
[2] J.K. Yoo, J. Kim, Y.S. Jung and K. Kang // *Adv. Mater*. **24** (2012) 5452.
[3] T. Song, J. Xia, J.H. Lee, D.H. Lee, M.S. Kwon and J.M. Choi // *Nano Lett.* **10** (2010) 1710.
[4] Y.H. Tang, L.Z. Pei, Y.W. Chen and C. Guo // *Phys. Rev. Lett.* **95** (2005) 019905.
[5] J. Bai, X.C. Zeng, H. Tanaka and J.Y. Zeng // *Proc. Natl. Acad. Sci. U. S. A.* **101** (2004) 2664.
[6] C.K. Chan, H. Peng, G. Liu, K. McIlwrath, X.F. Zhang and R.A. Huggins // *Nat. Nanotechnol.* **3** (2008) 31.
[7] Y. Wu, Y. Cui, L. Huynh, C.J. Barrelet, D.C. Bell and C.M. Lieber // *Nano Lett.* **4** (2004) 433.
[8] A.I. Boukai, Y. Bunimovich, J. Tahir-Kheli, J.-K. Yu, W.A. Goddard and J.R. Heath // *Nature* **451** (2008) 168.
[9] Y. Qu, H. Zhou and X. Duan // *Nanoscale* **3** (2011) 4060.
[10] Y.-S. Sohn, J. Park, G. Yoon, J. Song, S.-W. Jee and J.-H. Lee // *Nanoscale Res. Lett.* **5** (2009) 211.
[11] K. Seo, M. Wober, P. Steinvurzel, E. Schonbrun, Y. Dan and T. Ellenbogen // *Nano Lett.* **11** (2011) 1851.
[12] Y. Qu, L. Liao, Y. Li, H. Zhang, Y. Huang and X. Duan // *Nano Lett.* **9** (2009) 4539.
[13] A.T. Heitsch, C.M. Hessel, V. A. Akhavan and B. A. Korgel // *Nano Lett.* **9** (2009) 3042.
[14] X. Lu, C.M. Hessel, Y. Yu, T.D. Bogart and B. A. Korgel // *Nano Lett.* **13** (2013) 3101.
[15] O. El-Atwani, S. Ortoleva, A. Cimaroli and J.P. Allain // *Nanoscale Res. Lett.* **6** (2011) 403.
[16] B.K. Teo, X.H. Sun, T.F. Hung, X.M. Meng, N.B. Wong and S.T. Lee // *Nano Lett.* **3** (2003) 1735.
[17] G. Tai, K. Wang, Z. Sun, J. Yin, S.M. Ng and J. Zhou // *J. Phys. Chem. C.* **116** (2012) 532.
[18] P.R. Pudasaini, F. Ruiz-Zepeda, M. Sharma, D. Elam, A. Ponce and A.A. Ayon // *ACS Appl. Mater. Interfaces* **5** (2013) 9620.
[19] B. Kiraly, S. Yang and T.J. Huang // *Nanotechnology* **24** (2013) 245704.
[20] W. Gerberich, W. Mook, C. Perrey, C. Carter, M. Baskes and R. Mukherjee // *J. Mech. Phys. Solids.* **51** (2003) 979.
[21] H. Ma, F. Cheng, J. Chen, J. Zhao, C. Li and Z. Tao // *Adv. Mater.* **19** (2007) 4067.
[22] Y. Lu and A. Lal // *Nano Lett.* **10** (2010) 4651.
[23] Y.H. Wang, Y. He, R.J. Xiao, H. Li, K.E. Aifantis and X.J. Huang // *J. Power Sources* **202** (2012) 236.

[24] X.P. A Gao, G. Zheng and C.M. Lieber // *Nano Lett.* **10** (2010) 547.
[25] A. Zhang, H. Kim, J. Cheng and Y.-H. Lo // *Nano Lett.* **10** (2010) 2117.
[26] L. Wang, V. Reipa and J. Blasic // *Bioconjug. Chem.* **15** (2004) 409.
[27] P. Kale, A.C. Gangal, R. Edla and P. Sharma // *Int. J. Hydrogen Energy* **37** (2012) 3741.
[28] S.T. Kim, D.J. Kim, T.J. Kim, D.W. Seo, T.H. Kim and S.Y. Lee // *Nano Lett.* **10** (2010) 2877.
[29] Y. Yao, M.T. McDowell, I. Ryu, H. Wu, N. Liu, L. Hu, W.D. Nix and Y. Cui // *Nano Lett.* **11** (2011) 2949.
[30] W. Wang, Z. Favors, R. Ionescu, R. Ye, H.H. Bay, M. Ozkan and C.S. Ozkan // *Scientific reports* **5** (2015) 8781.
[31] K. Tang, L. Fu, R.J. White, L. Yu, M.M. Titirici and M. Antonietti // *Adv. Energy Mater.* **2** (2012) 873.
[32] R.J. White, K. Tauer, M. Antonietti and M.M. Titirici // *J. Am. Chem. Soc.* **132** (2010) 17360.
[33] M. Li, Q. Wu, M. Wen and J. Shi // *Nanoscale Res. Lett.* **4** (2009) 1365.
[34] Y.H. Ng, S. Ikeda, T. Harada, S. Higashida, T. Sakata and H. Mori // *Adv. Mater.* **19** (2007) 597.
[35] X.W. Lou, Y. Wang, C. Yuan, J.Y. Lee and L.A. Archer // *Adv. Mater.* **18** (2006) 2325.
[36] X.W. Lou, C.M. Li and L.A. Archer // *Adv. Mater.* **21** (2009) 2536.
[37] S. Ding, J.S. Chen, G. Qi, X. Duan, Z. Wang and E.P. Giannelis // *J. Am. Chem. Soc.* **133** (2011) 21.
[38] X. Zhou, Y.-X. Yin, L.-J. Wan and Y.-G. Guo // *J. Mater. Chem.* **22** (2012) 17456.
[39] S.F. Wang, F. Gu and M.K. Lü // *Langmuir* **22** (2006) 398.
[40] Y. Ding, X. Liu and R. Guo // *Colloids Surfaces A Physicochem. Eng. Asp.* **296** (2007) 8.
[41] H.-Y. Tuan, A. Ghezelbash and B.A. Korgel // *Chem. Mater.* **20** (2008) 2306.
[42] F. Mazen, T. Baron, A.M. Papon, R. Truche and J.M. Hartmann // *Appl. Surf. Sci.* **214** (2003) 359.
[43] Y. Yao, M.T. McDowell, I. Ryu, H. Wu, N. Liu and L. Hu // *Nano Lett.* **11** (2011) 2949.
[44] P.I. Ravikovitch, G.L. Haller and A. V. Neimark // *Adv. Colloid Interface Sci.* **76-77** (1998) 203.
[45] D. Ma, M. Li, A.J. Patil and S. Mann // *Adv. Mater.* **16** (2004) 1838.
[46] Z.F. Li, M.T. Swihart and E. Ruckenstein // *Langmuir* **20** (2004) 1963.
[47] R. A Bley, S.M. Kauzlarich, J.E. Davis and H.W.H. Lee // *Chem. Mater.* **8** (1996) 1881.
[48] L.L. Pang, J.Q. Bi, Y.J. Bai, H.L. Zhu, Y.X. Qi and C.G. Wang // *J. Phys. Chem. C.* **112** (2008) 12134.